Available online at www.sciencedirect.com
ScienceDirect
Lithos 96 (2007) 436–452
LITHOS
www.elsevier.com/locate/lithos

Late Triassic granitoids of the eastern margin of the Tibetan Plateau: Geochronology, petrogenesis and implications for tectonic evolution

L. Xiao [a,*], H.F. Zhang [a], J.D. Clemens [b], Q.W. Wang [c], Z.Z. Kan [c], K.M. Wang [c], P.Z. Ni [a], X.M. Liu [d]

[a] Faculty of Earth Science, China University of Geosciences, 388 Lumo Rd, Hongshan District, Wuhan 430074, China
[b] School of Earth Sciences & Geography, CEESR, Kingston University, Penrhyn Rd, Kingston-upon-Thames, Surrey KT1 2EE, UK
[c] Geological Survey Party of Sichuan Province, Chengdu 61500, China
[d] Key Laboratory of Continental Dynamics, Ministry of Education, Northwest University, Xi'an 710069, China

Received 11 January 2006; accepted 15 November 2006
Available online 13 March 2007

Abstract

Late Triassic granitoids in the Songpan-Garzê Fold Belt (SGFB), on the eastern margin of the Tibetan Plateau, formed at 230 to 220 Ma and can be divided into two groups. Group 1 are high-K calc-alkaline rocks with adakitic affinities (K-adakites), with Sr>400 ppm, Y<11 ppm, strongly fractionated REE patterns ($(La/Yb)_N$=32–105) and high K_2O/Na_2O (≈1). Group 2 are ordinary high-K calc-alkaline I-types with lower Sr (<400 ppm), higher Y (>18 ppm) and weakly fractionated REE patterns ($(La/Yb)_N$<20). Rocks of both groups have similar negative Eu anomalies (Eu/Eu*=0.50 to 0.94) and initial $^{87}Sr/^{86}Sr$ (0.70528 to 0.71086), but group 1 rocks have higher $\varepsilon_{Nd}(t)$ (−1.01 to −4.84) than group 2 (−3.11 to −6.71). Calculated initial Pb isotope ratios for both groups are: $^{206}Pb/^{204}Pb$=18.343 to 18.627, $^{207}Pb/^{204}Pb$=15.610 to 15.705 and $^{208}Pb/^{204}Pb$=38.269 to 3759. Group 1 magmas were derived through partial melting of thickened and then delaminated TTG-type, eclogitic lower crust, with some contribution from juvenile enriched mantle melts. Group 2 magmas were generated by partial melting of shallower lower crustal rocks. The inferred magma sources of both groups suggest that the basement of the SGFB was similar to the exposed Kangding Complex, and that the SGFB was formed in a similar manner to the South China basement. Here, passive margin crust was greatly thickened and then delaminated, all within a very short time interval (~20 Myr). Such post-collisional crustal thickening could be the tectonic setting for the generation of many adakitic magmas, especially where there is no spatial and temporal association with subduction.
© 2006 Elsevier B.V. All rights reserved.

Keywords: granite; K-adakite; geochronology; geochemistry; isotopes; songpan-garzê; Tibetan Plateau

1. Introduction

The eastern margin of the Tibetan Plateau experienced extensive plate collision and crustal deformation since the Late Triassic, and records the convergence between the Indian and Eurasian plates. This area has been called the "Asian puzzle" (Enkin et al., 1992) because it is one of the most important windows through which we can examine the processes of continental collision, magmatism and basin evolution. The huge triangular area of the Songpan-Garzê Fold Belt (Fig. 1) has attracted much attention over the past decade because it is located at the junction

* Corresponding author. Tel.: +86 27 6788 3048; fax: +86 27 6788 4711.
E-mail address: longxiao@cug.edu.cn (L. Xiao).

0024-4937/$ - see front matter © 2006 Elsevier B.V. All rights reserved.
doi:10.1016/j.lithos.2006.11.011

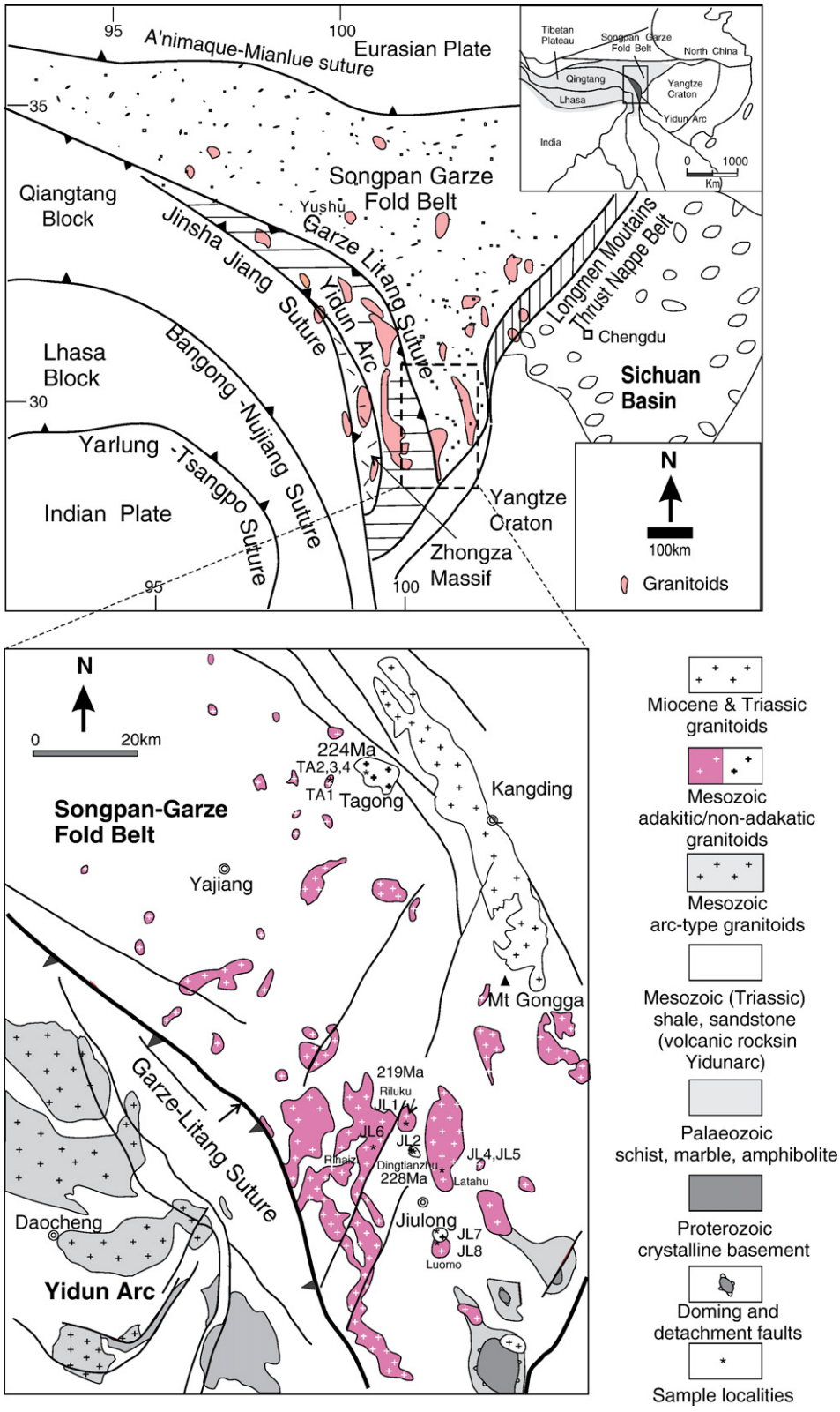


Fig. 1. Simplified geological map of the eastern margin of the Tibetan Plateau, modified from Roger et al. (1995), Ma (2002) and Reid et al. (in press). Shaded areas are granitoids. Inset is a regional geological map.

Table 1
LA-ICP-MS zircon analytical data for granitoids from the southern SGFB

Sample	Pb, ppm	Th, ppm	U, ppm	Th/U	$^{206}Pb/^{204}Pb$	$^{207}Pb/^{206}Pb$, 2σ	$^{206}Pb/^{238}U$, 2σ	$^{207}Pb/^{235}U$, 2σ	$^{207}Pb/^{206}Pb$, *t*/Ma (2σ)	$^{206}Pb/^{238}U$, *t*/Ma (2σ)	$^{207}Pb/^{235}U$, *t*/Ma (2σ)
Tagong biotite quartz diorite											
TA4-111	4	166	319	0.52	137	0.052±2	0.036±1	0.255±7	292±38	226±4	272±5
TA4-112	2	64	158	0.41	91	0.051±2	0.036±1	0.247±8	231±47	225±4	242±4
TA4-113	2	99	261	0.38	110	0.051±2	0.034±1	0.239±8	244±42	218±4	247±3
TA4-114	5	196	352	0.56	76	0.050±2	0.036±0	0.248±10	209±66	226±3	225±4
TA4-115	3	109	207	0.53	76	0.054±2	0.035±1	0.262±12	231±71	224±4	281±4
TA4-116	2	101	230	0.44	41	0.054±2	0.035±0	0.260±10	379±66	221±3	235±4
TA4-117	5	234	360	0.65	104	0.055±2	0.036±1	0.256±8	400±42	227±4	222±7
TA4-118	3	146	289	0.51	50	0.054±2	0.035±0	0.261±10	379 ±61	221±3	235±4
TA4-119	5	229	352	0.65	164	0.050±2	0.036±1	0.233±8	213±48	226±4	317±5
TA4-120	3	122	289	0.42	139	0.054±2	0.035±1	0.249±8	354±41	221±4	228±7
TA4-121	3	145	293	0.49	56	0.054±2	0.035±0	0.258±8	352±51	222±3	233±3
TA4-122	3	121	271	0.45	55	0.051±2	0.036±0	0.250±12	235±86	226±3	227±5
TA4-223	4	129	274	0.47	31	0.073±2	0.033±0	0.335±7	1022±48	210±2	293±6
Dingtianzhu quartz monzonite											
JL2-01	4	154	243	0.64	60	0.053±4	0.034±1	0.246±17	336±121	213±4	223±14
JL2-02	8	349	562	0.62	142	0.049±2	0.037±1	0.248±9	151±58	232±4	225±8
JL2-03	6	289	308	0.94	70	0.0510±3	0.036±1	0.250±13	233±90	226±4	227±11
JL2-04	4	154	169	0.91	35	0.053±4	0.037±1	0.267±20	316±138	232±5	240±17
JL2-05	4	159	218	0.73	60	0.051±4	0.035±1	0.246±15	217±109	224±4	223±13
JL2-06	4	175	181	0.96	32	0.052±4	0.036±1	0.259±20	291±134	228±5	234±16
JL2-07	4	172	226	0.76	54	0.050±3	0.036±1	0.247±13	193±93	227±4	224±11
JL2-08	4	182	260	0.7	46	0.051±4	0.036±1	0.252±17	251±116	226±4	228±13
JL2-09	5	224	332	0.68	79	0.052±3	0.033±1	0.241±14	303±98	211±4	219±11
JL2-10	1	58	104	0.56	18	0.051±5	0.037±1	0.259±25	257±181	232±5	234±21
JL2-11	2	105	136	0.77	29	0.057±4	0.036±1	0.279±17	483±103	226±4	250±14
JL2-12	7	303	329	0.92	72	0.051±2	0.036±1	0.250±9	224±61	227±4	226±8
JL2-13	5	223	406	0.55	32	0.068±4	0.031±1	0.292±14	872±70	197±4	260±11

JL2-14	6	257	410	0.63	98	0.051±2	0.036±1	0.255±9	251±52	229±4	231±7
JL2-15	6	266	452	0.59	107	0.050±2	0.037±1	0.253±8	209±49	231±4	229±7
JL2-16	5	244	255	0.96	63	0.052±3	0.035±1	0.252±14	273±91	224±4	228±11
JL2-17	6	280	321	0.87	80	0.051±3	0.036±1	0.256±11	243±70	230±4	231±9
JL2-18	5	215	349	0.62	29	0.067±6	0.031±1	0.288±23	837±129	198±5	257±19
JL2-19	6	239	280	0.85	48	0.066±4	0.038±1	0.350±15	820±62	242±4	305±12
JL2-20	5	202	295	0.69	65	0.052±3	0.037±1	0.265±12	275±73	235±4	239±10
Riluku K-adakite											
JL1-01	4	173	520	0.33	115	0.052±6	0.034±1	0.241±24	271±180	214±5	219±20
JL1-02	8	393	749	0.52	86	0.050±4	0.035±1	0.238±19	185±139	220±5	217±±16
JL1-03	4	160	513	0.31	80	0.052±5	0.035±1	0.250±22	263±159	223±5	227±18
JL1-04	4	210	653	0.32	102	0.050±7	0.034±1	0.233±32	212±144	213±7	213±26
JL1-05	5	244	581	0.42	100	0.051±5	0.036±1	0.254±23	259±166	227±5	230±19
JL1-06	4	171	496	0.35	94	0.052±5	0.036±1	0.257±21	276±144	228±5	232±17
JL1-07	4	189	598	0.32	104	0.053±7	0.035±1	0.257±23	335±160	222±5	232±19
JL1-08	3	149	481	0.31	48	0.052±7	0.034±1	0.244±30	291±222	215±5	221±24
JL1-09	2	109	364	0.3	74	0.054±5	0.034±1	0.254±32	379±227	216±6	230±26
JL1-10	4	173	469	0.37	78	0.051±6	0.035±1	0.244±21	250±145	219±7	221±16
JL1-11	5	210	463	0.46	95	0.068±6	0.041±1	0.380±31	855±122	258±5	327±22
JL1-12	4	188	531	0.35	82	0.051±5	0.034±1	0.235±21	221±157	213±6	214±17
JL1-13	4	182	475	0.38	68	0.051±7	0.036±1	0.250±31	231±220	226±7	226±25
JL1-14	3	128	418	0.31	88	0.050±6	0.035±1	0.240±27	208±191	219±6	218±21
JL1-15	12	309	746	0.41	216	0.055±4	0.059±1	0.452±26	420±98	372±7	379±19
JL1-16	2	109	353	0.31	67	0.052±7	0.035±1	0.249±35	262±252	223±7	226±28
JL1-17	10	466	935	0.5	133	0.055±5	0.033±1	0.249±22	415±150	208±5	226±17
JL1-18	7	215	656	0.33	106	0.058±6	0.048±1	0.381±34	527±151	300±8	328±25
JL1-19	10	497	718	0.69	115	0.054±5	0.034±1	0.252±21	366±146	215±5	228±17
JL1-20	7	303	765	0.4	109	0.051±4	0.035±1	0.245±15	245±106	221±4	223±12

between three lithospheric plates; the South China Block, the North China Block and the Tibetan Plateau (Enkin et al., 1992; Mo et al., 1993; Xu et al., 2002; Hou et al., 2004; Reid et al., 2005; Harrowfield and Wilson, 2005). In response to the tectonic events, magmatism was extensive throughout the evolution of the area, especially in the Late Palaeozoic and Early Mesozoic. Recent geochronological (Roger et al., 2004; Zhang et al., 2006) and geochemical (BGMR of Sichuan, 1990; Zhang et al., 2006) studies suggest that most of the magmas formed during the Indosinian Orogeny (Sengör, 1984; Yin and Nie, 1993). Tectonically, this orogen is composed of an eastern, major Songpan-Garzê Fold Belt (SGFB) and a southwestern, minor Yidun arc (Xu et al., 1992; Reid et al., 2005) separated by the Garzê-Litang suture (Fig. 1).

Zhang et al. (2006) studied two granitoids from the northern SGFB and identified them adakitic. This shows that adakitic magmas were developed in the eastern margin of the Tibetan Plateau in the Early Mesozoic (around 210 to 220 Ma). There are no previous records of adakites in this area or in this time period. This raises a series of questions about their petrogenesis and tectonic setting. This paper presents the geochronology, geochemistry and Sr–Nd–Pb isotopic compositions of eight more granitoid bodies from the southern SGFB, with the aim of clarifying their age, petrogenesis and tectonic significance. In the course of the study, we identified two distinct groups of granitoids — adakitic and ordinary I-type granitoids. This is the first report of coeval adakitic and ordinary, high-K, I-type, calc-alkaline granitoids in same tectonic setting. Thus, our data provide new insights into the magmatic processes as well as the structure of the crust.

2. Geological setting and samples

The SGFB is bounded by the Yangtze (South China), North China and North Tibet (Qiangdam) continental Blocks (Fig. 1). To the east, the Longmenshan Thrust-nappe belt separates the SGFB from the Sichuan basin (Xu et al., 1992; Chen et al., 1995; Chen and Wilson, 1996). The northern limit of the SGFB is marked by the A'nimaque-Mianlue suture zone, which is considered to be a Late Palaeozoic Palaeo-Tethys oceanic subduction zone dipping to the north (Sun et al., 2002; Xu et al., 2002; Elena et al., 2003). To the southwest, the SGFB is bounded by the Garzê-Litang suture zone, which is also considered to be a Late Palaeozoic Palaeo-Tethys oceanic subduction zone, dipping either to the west (Sengör, 1985; Hou et al., 2004; Reid et al., 2005) or the east (Calassou, 1994). In the SGFB, the sediments are almost exclusively Triassic marine flysch deposits that reach a thickness of 5 to 15 km (Xu et al., 1992; Calassou, 1994). The Triassic flysch sediments were intensely folded during the Indosinian (Late Triassic) compressional tectonism due to convergence between the North China, Yangtze and Qiangtan continental blocks (Xu et al., 1992; Bruguier et al., 1997). A large décollement near the eastern and southeastern margin of the Songpan-Garzê basin separates the Triassic flysch and the Palaeozoic sedimentary cover and the crystalline basement of the Yangtze block (Mattauer et al., 1992; Xu et al., 1992; Calassou, 1994). Recent work has suggested that the basement of the Songpan-Garzê belt would once have been a peninsula approaching the Palaeo-Tethys Ocean from the Yangtze block (Zhang et al., 2006, in press).

Granitoids are widespread in the SGFB (Fig. 1), most of them having sharp intrusive contacts with the Triassic sediments. Published U–Pb zircon and Rb–Sr whole-rock ages of granitoids from the southern parts of the SGFB range from 230 to 190 Ma (BGMR of Sichuan, 1990; Reid et al., in press). In the northern part of the SGFB, U–Pb zircon ages are 220 to 210 Ma (Qin et al., 2005; Zhang et al., 2006). These dates imply that the magmatism was generally coeval with the Indosinian Orogeny.

In the southern part of the SGFB, several granitoid intrusions (Riluku, Dingtianzhu, Rihaizi, Latahu and Luomo) cluster around Jiulong (Fig. 1). Most show similar petrographic characteristics and have been grouped together as parts of the same batholith (BGMR of Sichuan, 1990). Field outcrop and thin-section petrographic observations show that these porphyritic granitoids (samples JL1, JL4 to JL6 and JL8) contain between 5 and 15% of plagioclase and K-feldspar phenocrysts. Major minerals are plagioclase (40 to 55%), K-feldspar (20 to 35%), biotite (2 to 10%), quartz (5 to 25%) and hornblende (1 to 5%). Accessory minerals are zircon, apatite, magnetite and titanite. Two small outcrops of rocks with higher hornblende contents (5 to 10%) were also sampled (JL2 and JL7), to determine their relationships to the more felsic rocks. To the north is the Tagong intrusion, composed of a western quartz monzonite and an eastern monzonite; these were also sampled. The small quartz monzonite (TA1) contains plagioclase (45%), K-feldspar (30%), biotite (10%) and quartz (15%). The eastern monzonite (samples TA2 to TA4) contains up to 10% hornblende, similar to samples JL2 and JL7.

3. Analytical methods

Eleven samples (Fig. 1) were chosen for geochemical and isotopic analysis. At the Key Laboratory of

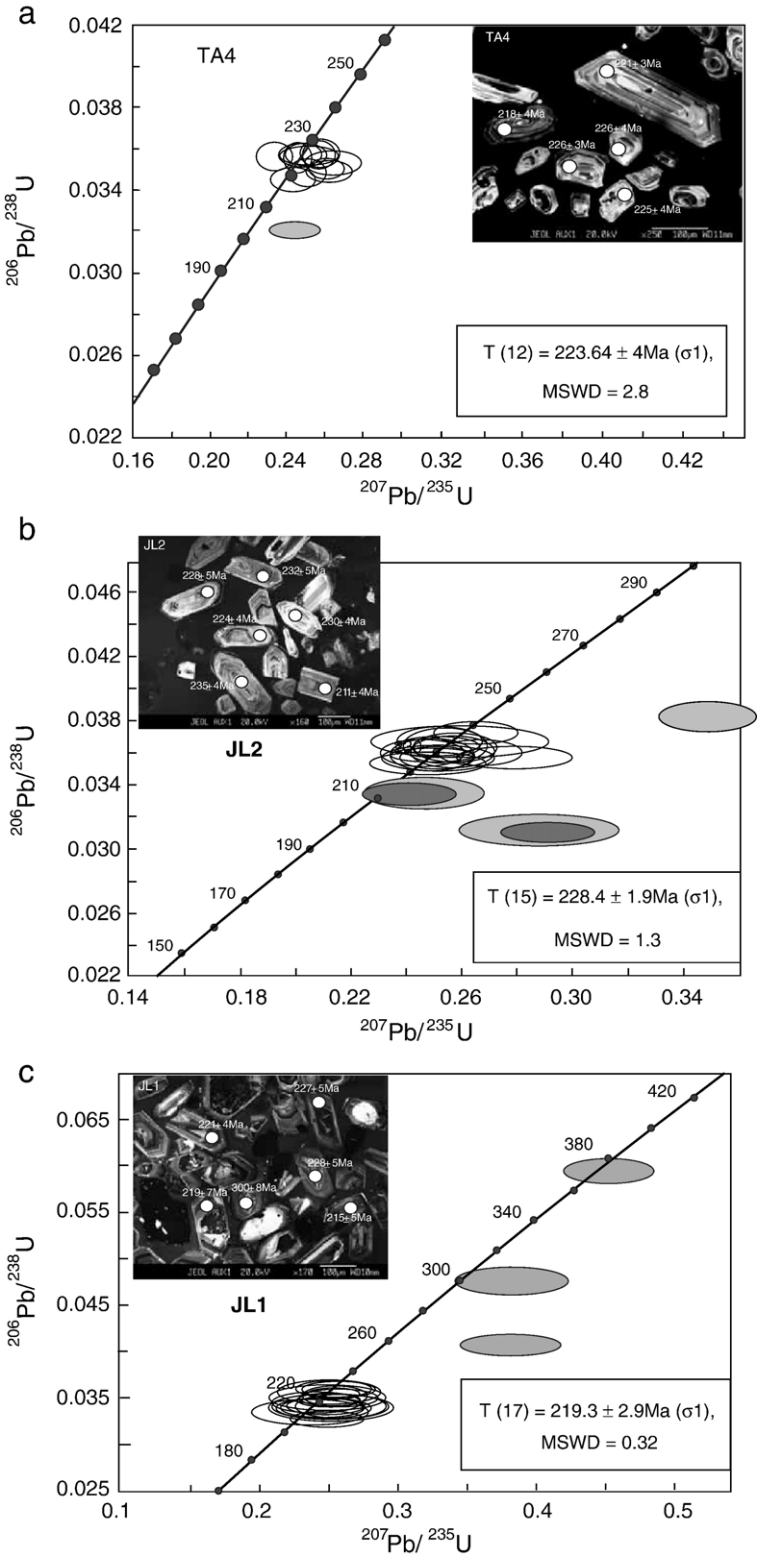


Fig. 2. CL images and U–Pb concordia diagrams for the Tagong (TA4), south Riluku (JL2) and Riluku (JL1) granitoids.

Table 2
Compositions of granitoids on the eastern margin of the Tibetan Plateau

Group 1							Group 2				
Intrusion	Riluku	North Latahu	North Ladahu	Rihaizi	South Luomo	West Tagong	Tagong	Tagong	Tagong	Dingtianzhu	North Luomo
Sample	JL1	JL4	JL5	JL6	JL8	TA1	TA2	TA3	TA4	JL2	JL7
wt.%											
SiO_2	68.13	69.66	71.49	64.91	72.07	71.59	61.75	62.68	59.65	61.56	65
TiO_2	0.33	0.44	0.39	0.63	0.3	0.31	0.72	0.64	0.72	0.69	0.65
Al_2O_3	16.63	15.79	14.56	15.68	14.89	14.87	16.09	15.71	16.07	16.61	16.46
FeO*	2.29	2.10	2.18	4.46	1.53	2.19	6.16	5.23	6.16	4.76	4.86
MgO	0.79	0.59	0.42	1.91	0.48	0.49	3.42	2.71	3.61	1.95	1.73
MnO	0.05	0.04	0.04	0.1	0.03	0.03	0.12	0.1	0.12	0.11	0.1
CaO	2.83	2.15	1.46	4.5	1.56	2.44	5.04	4.8	5.97	5.06	5.19
K_2O	3.81	4.5	5.03	3.32	4.94	2.37	3.73	3.87	3.46	3.73	2.27
Na_2O	4.16	4.28	3.43	3.9	3.1	4.42	1.95	2.07	2.12	3.39	2.5
P_2O_5	0.09	0.1	0.08	0.33	0.1	0.11	0.13	0.12	0.15	0.35	0.12
LOI	0.18	0.21	0.78	0.66	0.54	0.48	0.79	0.65	0.12	0.48	0.6
Total	100.59	99.86	99.86	100.4	99.54	99.30	99.9	98.58	99.15	98.69	99.48
A/CNK	1.03	1.00	1.06	0.86	1.12	1.04	0.98	0.96	0.89	0.88	1.03
K_2O/Na_2O	0.92	1.05	1.47	0.85	1.59	0.54	1.91	1.87	1.63	1.10	0.91
Mg#	40	35	27	45	37	30	51	50	53	44	40
ppm											
Sc	3.56	2.88	2.68	2.64	2.75	2.86	17.13	13.67	21.32	10.01	12.94
V	22.01	17.12	13.34	12.65	12.03	14.77	101.20	80.21	138.60	65.84	47.28
Cr	21.71	9.59	31.90	29.27	11.70	30.73	130.80	53.56	62.06	38.12	176.30
Co	4.02	3.01	2.42	2.39	1.95	2.61	16.86	13.22	19.94	9.23	8.64
Ni	6.10	2.35	10.14	9.43	3.62	11.05	41.41	16.07	13.56	49.95	16.67
Ga	19.71	23.34	21.47	20.94	21.29	20.77	16.32	16.06	16.24	20.54	17.21
Ge	1.21	1.02	1.58	1.58	1.28	1.05	1.84	1.64	1.90	1.57	1.67
Rb	170	150	211	209	211	105	142	159	186	140	79
Sr	570	812	475	467	410	376	226	219	217	956	335
Y	7.4	8.8	10.7	10.9	7.9	4.7	22.9	24.9	24.4	19.2	18.5
Zr	155	249	242	237	164	88	147	133	123	261	94
Nb	30.1	20.1	20.9	21.0	13.5	15.4	13.5	14.6	16.0	24.5	13.6
Ba	868	1348	1258	1245	1003	518	676	610	448	1507	510
La	30.10	76.23	84.52	83.46	51.37	48.97	23.05	25.13	19.72	47.80	28.27
Ce	52.82	133.10	145.50	142.40	88.71	82.73	40.73	50.99	40.38	88.34	55.47
Pr	5.52	13.94	15.31	15.44	9.47	8.79	6.06	6.23	5.68	10.33	6.95
Nd	17.80	41.88	47.17	45.74	30.19	25.86	22.07	22.91	22.43	35.62	24.40
Sm	2.89	5.69	6.17	6.22	4.53	3.32	4.61	4.70	5.16	6.09	4.66
Eu	0.76	1.08	0.80	0.86	0.66	0.61	0.89	0.84	0.88	1.53	1.02
Gd	1.85	2.46	3.04	2.94	2.14	1.58	3.75	3.93	4.53	4.17	3.31
Tb	0.28	0.40	0.47	0.50	0.36	0.23	0.66	0.69	0.76	0.64	0.57
Dy	1.47	1.76	2.23	2.25	1.61	0.99	3.93	4.37	4.44	3.50	3.12
Ho	0.27	0.30	0.37	0.38	0.25	0.17	0.81	0.87	0.92	0.65	0.64
Er	0.73	0.80	0.96	1.02	0.65	0.44	2.25	2.33	2.37	1.72	1.73
Tm	0.11	0.10	0.13	0.14	0.08	0.05	0.34	0.38	0.34	0.26	0.27
Yb	0.67	0.65	0.79	0.85	0.53	0.34	2.24	2.40	2.21	1.73	1.66
Lu	0.11	0.09	0.11	0.13	0.07	0.05	0.36	0.38	0.36	0.29	0.27
Hf	4.41	6.06	5.99	5.86	4.12	2.41	4.20	3.81	3.13	6.31	2.63
Ta	1.86	1.16	1.51	1.59	1.18	0.56	1.02	1.23	1.14	1.27	0.97
Th	17.39	23.94	27.34	27.40	20.88	17.99	7.24	15.04	9.13	17.93	10.24
U	3.33	2.72	2.58	3.17	2.02	1.68	1.52	3.35	1.53	3.94	2.07
Sr/Y	77	92	44	43	52	80	10	9	9	50	18
La/YbN	32	85	77	71	70	105	7	8	6	20	12
Eu/Eu*	0.94	0.76	0.50	0.54	0.57	0.71	0.63	0.58	0.54	0.88	0.76

*total Fe as FeO.

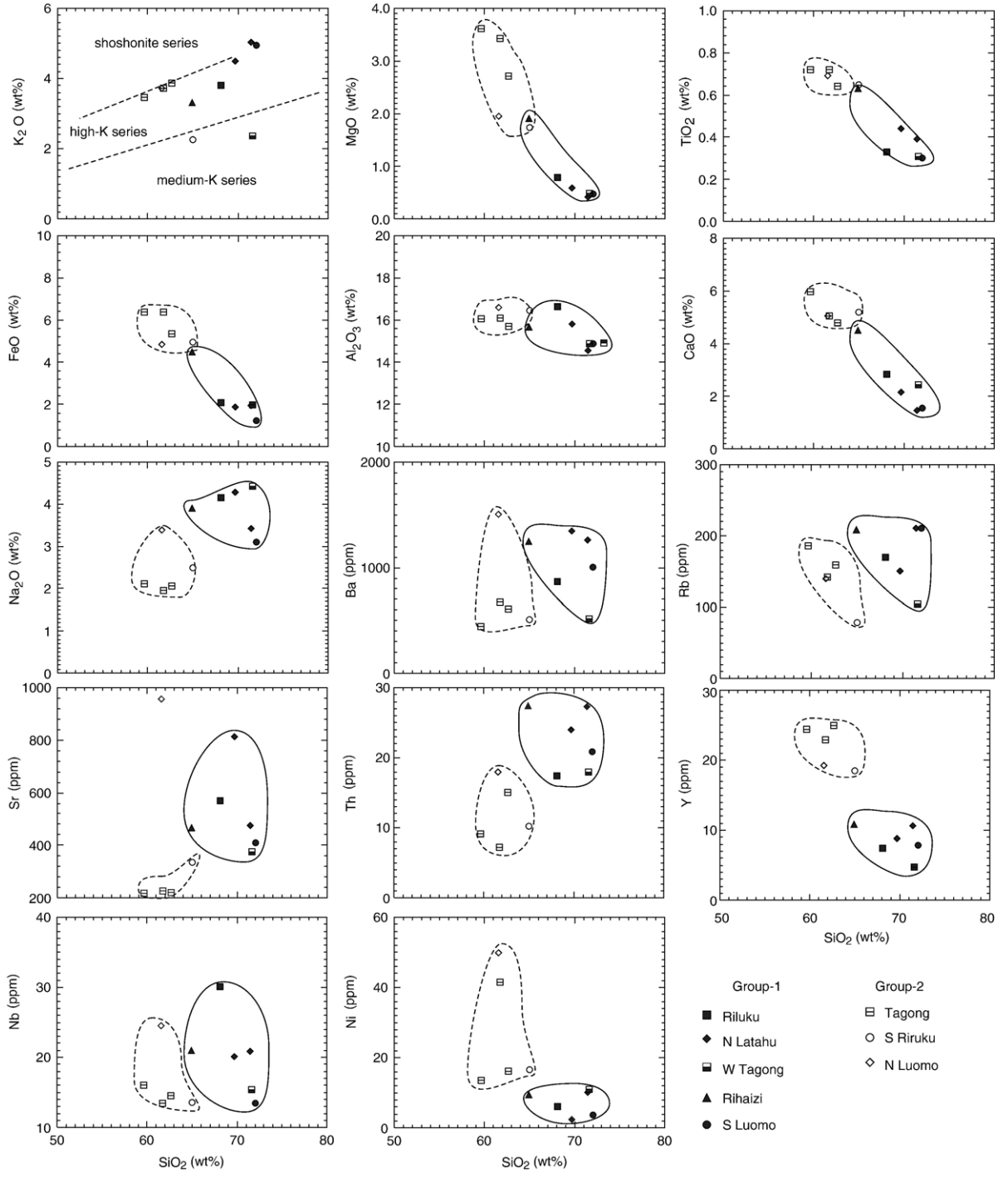


Fig. 3. Harker variation diagrams for the Late Triassic granitoids from the Songpan-Garzê Fold Belt. Solid lines enclose the fields for group 1 K-adakites and dashed lines for the group 2 ordinary I-type granitoids.

Continental Dynamics, Ministry of Education, Northwest University, China, zircons from three granitoids (TA4, JL2 and JL1) were dated, using the U–Pb system and LA-ICP-MS methods (Yuan et al., 2004). Elemental and other isotopic analyses were carried out at the Guangzhou Institute of Geochemistry, China Academy of Sciences. Major-element compositions were analyzed by XRF, with an analytical uncertainty generally < 5%.

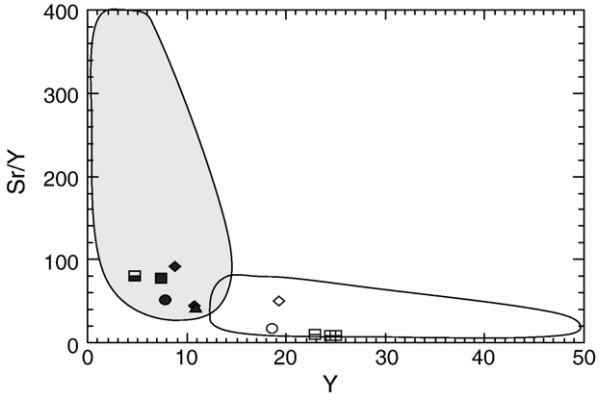


Fig. 4. Sr/Y versus Y plots for the granitoids from the Songpan-Garzê Fold Belt.

Trace elements and rare earth elements (REE) were measured using ICP-MS, with analytical precision better than 10%. For detailed analytical methods see Liu et al. (1996).

Whole-rock Sr–Nd isotope data were obtained using a Micromass Isoprobe MC-ICP-MS. Sr and Nd isotope fractionations were corrected to $^{86}Sr/^{88}Sr=0.1194$ and $^{146}Nd/^{144}Nd=0.7219$, respectively. Total procedural Sr and Nd blanks are <4 ng and <1 ng, respectively. Details of the methods are given in Liang et al. (2003). Whole-rock Pb was separated by anion exchange on HCl–Br columns. Pb isotope ratios were measured by Nu Plasma. Pb isotope fractionation was corrected to $^{205}Tl/^{203}Tl=2.3875$. Within the analytical period, thirty measurements of NBS981 gave average values of $^{206}Pb/^{204}Pb=16.937\pm1(1\sigma)$, $^{207}Pb/^{204}Pb=15.491\pm1$ and $^{208}Pb/^{204}Pb=36.696\pm1$. The BCR-2 standard gave $^{206}Pb/^{204}Pb=18.742\pm1$ (1σ), $^{207}Pb/^{204}Pb=15.620\pm1$ and $^{208}Pb/^{204}Pb=38.705\pm1$. Total procedural Pb blanks were in the range of 0.1 to 0.3 ng.

4. Results

4.1. U–Pb zircon ages

U–Pb zircon LA-ICP-MS data are given in Table 1, and representative zircon CL images and spot analyses are shown in Fig. 2. Zircons from the Tagong biotite quartz diorite (sample TA4) are pink to colourless, with well-developed crystal faces. Most have length/width ratios of 2 to 3. They have subtle magmatic oscillatory zoning (Fig. 2a) and lack inherited cores. Thirteen spot analyses show that they are mostly concordant but one age fall off the concordant line (Fig. 2a). The $^{206}Pb/^{238}U$ ages range from 218 to 226 Ma of 12 concordant spots, with an average of 223.6±4 Ma (1σ; MSWD=2.8). This is interpreted as the date of magma emplacement.

Zircons from the Dingtianzhu quartz monzonite (JL2) are dominated by light pink to colourless euhedral crystals with perfect pyramids and prisms. The zircons range in length from ~100 to ~250 μm with length/width ratios of 2 to 3. The zircon CL images (e.g. JL2 in Fig. 2b) exhibit oscillatory magmatic zoning, without inherited cores. Twenty spot analyses show that these zircons are mostly concordant within error (Fig. 2b). Fifteen concordant zircons have $^{206}Pb/^{238}U$ ages ranging from 235 to 224 Ma, with a weighted average of 228.4±1.9 Ma (1σ; MSWD=1.3), again interpreted as the age of magma emplacement.

Zircons from the Riluku biotite monzonitic granite (sample JL1) are colourless. Most zircons range in length from ~100 to 200 μm with length/width ratios from 1 to 2. Zircon CL images (Fig. JL1 in Fig. 2c) also exhibit oscillatory magmatic zoning but some have inherited cores. Seventeen analysed zircons from this granite have $^{206}Pb/^{238}U$ ages ranging from 208 to 228 Ma, with a weighted average of 219.3±2.9 Ma (1σ; MSWD=0.32). These ages lie on concordia (Fig. 2c) and represent the date of magma emplacement. The

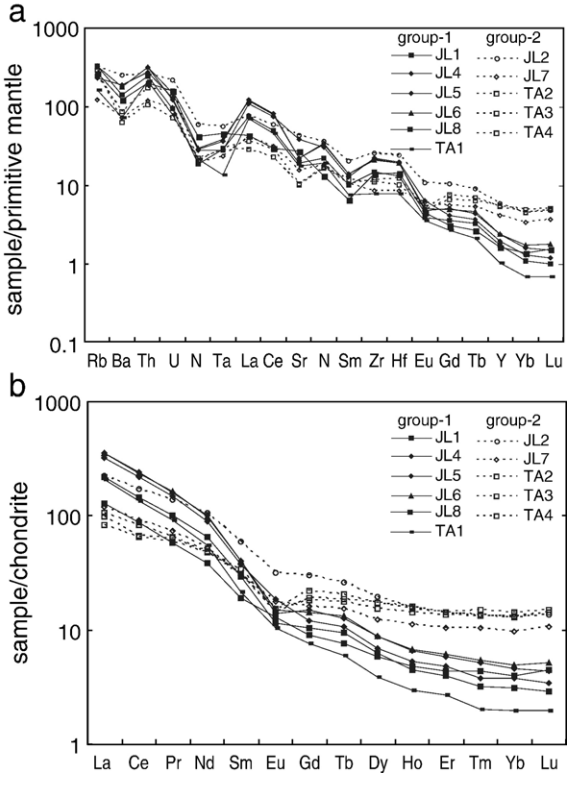


Fig. 5. Primitive-mantle–normalized multi-element diagrams and chondrite-normalised REE patterns.

Table 3
Nd and Sr isotope analyses of granitoids from the eastern margin of the Tibetan Plateau

Rock type	Intrusion	Sample no.	Rb (ppm)	Sr (ppm)	$^{143}Nd/^{144}Nd$	$^{87}Rb/^{86}Sr$	$(^{87}Sr/^{86}Sr)$ m±2σ	$^{87}Sr/^{86}Sr_i$	Sm (ppm)	Nd (ppm)	$^{147}Sm/^{144}Nd$	$\varepsilon_{Nd}(t)$[a]	T_{DM} (Ga)[b]
Group 1	Riluku	JL1	170	570	0.512441	0.863	0.70977±1	0.70701	2.89	17.8	0.098	−1.01	0.94
	Latahu	JL4	150	812	0.512250	0.536	0.70932±1	0.70760	5.69	41.88	0.082	−4.29	1.05
	Ladahu	JL5	211	475	0.512217	1.285	0.71136±1	0.70724	6.17	47.17	0.079	−4.84	1.06
	Rihaizi	JL6	209	467	0.512310	1.294	0.70911±1	0.70496	6.22	45.74	0.082	−3.12	0.98
	S Luomo	JL8	211	410	0.512205	1.490	0.71245±1	0.70769	4.53	30.19	0.091	−5.41	1.17
	W Tagong	TA1	105	376	0.512312	0.807	0.70758±1	0.70494	3.32	25.86	0.078	−2.87	0.94
Group 2	Tagong	TA2	142	226	0.512196	1.820	0.71312±1	0.70716	4.61	22.07	0.126	−6.56	1.66
	Tagong	TA3	159	219	0.512185	2.105	0.71418±1	0.70729	4.70	22.91	0.124	−6.71	1.64
	Tagong	TA4	186	217	0.512237	2.479	0.71495±1	0.70684	5.16	22.43	0.139	−6.14	1.87
	Dingtianzhu	JL2	203	956	0.512355	0.652	0.70843±1	0.70621	9.10	48.89	0.113	−3.11	1.20
	N Luomo	JL7	79	335	0.512223	0.683	0.71281±1	0.71062	4.66	24.4	0.115	−5.77	1.44

a and b: The $^{143}Nd/^{144}Nd$ and $^{147}Sm/^{144}Nd$ of chondrite and depleted mantle at present day are 0.512638 and 0.1967, 0.51315 and 0.222, respectively. $^{87}Sr/^{86}Sr_i$ and $\varepsilon_{Nd}(t)$ were calculated at 220 Ma.

other 3 older ages (258, 300 and 375 Ma) are discordant, indicating that the zircons contain inherited cores with loss of common Pb.

4.2. Major and trace element data

Major and trace element compositions of all samples are given in Table 2. These data suggest a significant variation in most major elements, as illustrated in Fig. 3. Granitoids from the SGFB have SiO_2 contents of 59.65 to 72.07 wt.%, MgO of 0.42 to 3.61 wt.% and total alkali (K_2O+Na_2O) contents of 5.94 to 8.78 wt.%. These characteristics show that these rocks form a high-K calc-alkaline series (Fig. 3). Their A/CNK values (mol. $Al_2O_3/(CaO+K_2O+Na_2O)$) are <1.1, except for sample JL8 (A/CNK=1.12) and would be classified as I-type granitoids.

On Harker variation diagrams (Fig. 3), all samples generally display Al_2O_3, CaO, FeO*, MgO, P_2O_5 and TiO_2 contents decreasing and K_2O contents increasing with increasing SiO_2 contents. Individual intrusions show different ranges of SiO_2 contents and other major oxides, suggesting that separate, distinct magma batches formed the different pluton.

Using the Harker diagrams in Fig. 3, the granitoids can be divided into two groups: group 1 rocks have higher Sr (mostly >400 ppm) and lower Y contents (4.7 to 10.9 ppm); group 2 granitoids have lower Sr (<335 ppm, with exception of JL2=956 ppm) and higher Y contents (18.5 to 24.9 ppm). These differences result in distinctive Sr/Y ratios (see Table 1 and Fig. 4). Group 1 granitoids have high Sr/Y ratios (43 to 92), and group 2 granitoids have low ratios (9 to 18, with the exception of JL2=50). The group 1 rocks have lower MgO, TiO_2, FeO*, CaO, Y and Ni, and higher SiO_2, Na_2O, Sr and Th contents than the group 2 granitoids (Fig. 3). In general, group 1 samples are monzogranites, while group 2 samples are monzodiorites, as described above.

Table 4
Whole-rock Pb isotope data

Rock type	Intrusion	Sample no	Pb (ppm)	Th (ppm)	U (ppm)	$^{206}Pb/^{204}Pb$ ±2σ	$^{207}Pb/^{204}Pb$ ±2σ	$^{208}Pb/^{204}Pb$ ±2σ	$(^{206}Pb/^{204}Pb)^*$	$(^{207}Pb/^{204}Pb)^*_t$	$(^{208}Pb/^{204}Pb)^*_t$
Group 1	Riluku	JL1	37.21	17.39	3.33	18.699±1	15.661±1	38.925±5	18.495	15.651	38.578
	Latahu	JL4	24.06	23.94	2.72	18.682±1	15.639±1	39.009±7	18.424	15.626	38.269
	Ladahu	JL5	25.38	27.34	2.58	18.774±1	15.622±1	39.099±4	18.542	15.610	38.297
	Rihaizi	JL6	25.6	27.40	3.17						
	S Luomo	JL8	31.59	20.88	2.02	18.774±1	15.704±1	39.102±10	18.627	15.697	38.609
	W Tagong	TA1	26.03	17.99	1.68						
Group 2	Tagong	TA2	22.38	7.24	1.52	18.699±1	15.625±1	38.766±6	18.545	15.617	38.527
	Tagong	TA3	24.39	15.04	3.35	18.845±1	15.709±1	39.038±3	18.530	15.693	38.578
	Tagong	TA4	17.6	9.13	1.53	18.548±1	15.646±1	38.778±5	18.350	15.636	38.394
	Dingtianzhu	JL2	27.38	17.93	3.94	18.733±1	15.663±1	39.027±6	18.343	15.643	38.420
	N Luomo	JL7	17.41	10.24	2.07	18.763±1	15.719±1	39.198±3	18.490	15.705	38.759

*Initial Pb isotopic ratio at t=220 Ma, calculated using single Pb isotopic evolutional model (Zartman and Doe, 1981).

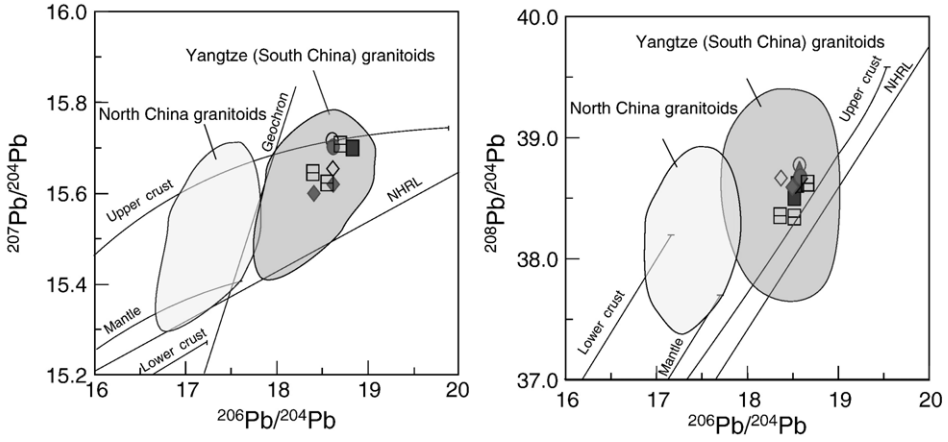


Fig. 6. (a) $^{207}Pb/^{204}Pb$ vs $^{206}Pb/^{204}Pb$ diagram, (b) $^{208}Pb/^{204}Pb$ vs $^{206}Pb/^{204}Pb$ diagram. K-feldspar Pb isotope ratios of Mesozoic granitoids for the North China and Yangtze granitoids are from Zhang (1995). Data for the SGFB and Yidun arc granitoids are whole-rock initial Pb isotope ratios (see Table 4). Pb isotopic evolution lines of upper crust, lower crust and mantle are from Zartman and Doe (1981).

The Sr/Y vs Y diagram (Fig. 4) is generally applied to distinguish adakitic from other calc-alkaline rocks (Defant and Drummond, 1990). In this diagram, group 1 rocks plot within the adakite field, while group 2 fall in the field for ordinary calc-alkaline granitoids. Additionally, group 1 rocks have geochemical and isotopic characteristics similar to rocks, in eastern China, that have high K_2O contents and high K_2O/Na_2O ratios, termed K-adakites or C-type adakites (Zhang et al., 2001; Rapp et al., 2002). Their origin and its geological implications will be discussed later, but see Xiao and Clemens (2007).

Group 1 and 2 granitoids show distinct primitive-mantle–normalized multi-element patterns (Fig. 5a). Group 1 are rich in large-ion lithophile elements (LILE), display steep arrays, falling away to the right of the diagram, and have negative Nb and Ta anomalies. Group 2 rocks have relatively flat patterns and have high Y and Yb contents. These differences are also apparent in the REE patterns (Fig. 5b). Group 1 display strongly fractionated REE patterns with $(La/Yb)_N > 32$ and negative Eu anomalies (Eu/Eu* = 0.50 to 0.94), suggesting the presence of garnet and some of plagioclase in their source rocks or a small degree of plagioclase fractionation. As is typical of calc-alkaline I-type granites (Chappell and White, 1974, 2001), group 2 rocks have relatively flat REE patterns with $(La/Yb)_N < 20$ and Eu/Eu* = 0.54–0.88.

4.3. Sr, Nd and Pb isotopes

As shown in Table 3, group 1 rocks have variable $^{87}Rb/^{86}Sr$ ratios (0.536 to 1.49) and present-day $^{87}Sr/^{86}Sr$ ratios (0.707578 to 0.712455). The initial $^{87}Sr/^{86}Sr$ ratios, calculated using the U–Pb zircon ages in Table 3, are <0.708. Group 2 rocks have higher $^{87}Rb/^{86}Sr$ ratios (0.65 to 2.48) and present-day $^{87}Sr/^{86}Sr$ ratios (0.708298 to 0.71495). Their initial $^{87}Sr/^{86}Sr$ ratios range from 0.70621 to 0.70729 (with exception of JL7 = 0.71062), overlapping with the values for the group 1 rocks.

Whole-rock Pb isotope data (Table 4) show that all SGFB granitoids have similar Pb isotope compositions (Fig. 6). Initial Pb isotope ratios were calculated using a single-stage Pb isotope evolution model (Zartman and Doe, 1981). Calculated initial Pb isotope ratios are $^{206}Pb/^{204}Pb = 18.343$ to 18.627, $^{207}Pb/^{204}Pb = 15.610$ to 15.705 and $^{208}Pb/^{204}Pb = 38.269$

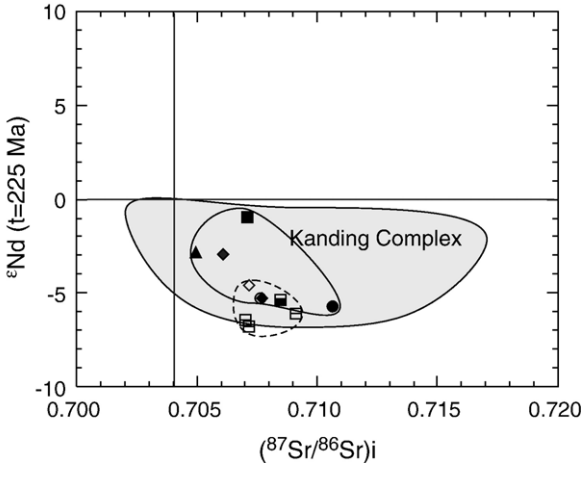


Fig. 7. Plot of $\varepsilon_{Nd}(t)$ vs initial $^{87}Sr/^{86}Sr$. Symbols as in Fig. 2.

to 38.759. The Pb isotope ratios of group 1 and 2 rocks are indistinguishable.

Among group 1 granitoids, $^{147}Sm/^{144}Nd$ ratios range from 0.078 to 0.098 and $\varepsilon_{Nd}(t)$ values from −1.01 to −5.41. In group 2 granitoids, $^{147}Sm/^{144}Nd$ ratios range from 0.113 to 0.139 and $\varepsilon_{Nd}(t)$ from −3.11 to −6.71. On the $\varepsilon_{Nd}(t)$ vs initial $^{87}Sr/^{86}Sr$ diagram (Fig. 7), group 1 and 2 granitoids can be distinguished only by the lower $\varepsilon_{Nd}(t)$ in group 2 rocks. See also Table 3.

5. Discussion

5.1. Magma evolution and petrogenesis

The geochemical and isotopic characteristics of the two coeval groups of I-type granitoids in the SGFB suggest that the magmas were generated from different source rocks and/or experienced contrasting processes of magma evolution.

Most of the major oxides in analyses of both group 1 and 2 granitoids show near-linear relationships with SiO_2 (Fig. 3). Their Sr and Pb isotope ratios also have similar broad ranges (Figs. 6 and 7). These characteristics could be interpreted to mean that the magmas for both groups had the same source but that they experienced different fractional crystallization (FC) or AFC (assimilation and FC) processes. If this were correct, we would expect corresponding consistent trace element, REE and isotopic variations. Such evolutionary processes might be identified from plots of Mg# vs $\varepsilon_{Nd}(t)$ and Nb/La vs $\varepsilon_{Nd}(t)$ (Fig. 8a,b). However, these plots suggest that neither FC nor AFC processes could generate the group 1 magmas from the group 2 magmas. Additionally, the trace element and REE patterns (Fig. 5) are not in accord such a model. Nevertheless, some FC probably occurred *within* each group of magmas (Fig. 8b,c,d). The Si/P vs (Fe+Mg)/P plot (Ernst et al., 1988) in Fig. 8c suggests that there was no significant fractionation of clinopyroxene in the group 2 magmas, but that plagioclase and/or clinopyroxene fractionation could have affected the compositions of the group 1 magmas. If the group 1 magmas had experienced plagioclase fractionation, they should

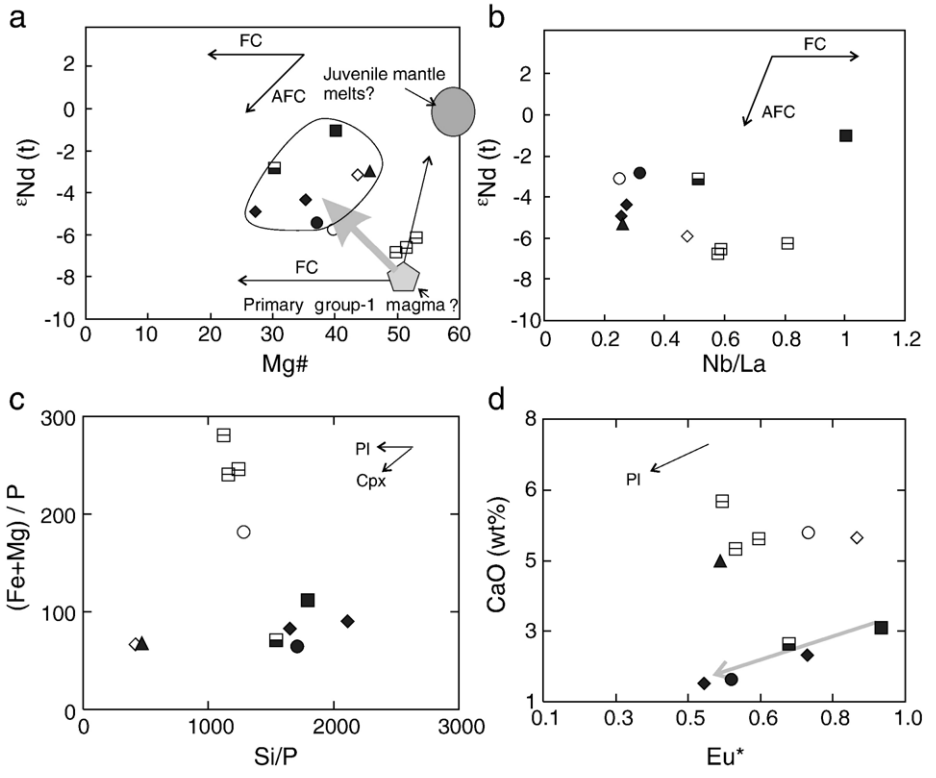


Fig. 8. Element and isotope plots to show potential fractional crystallization (FC) and assimilation fractional crystallization (AFC) processes. a. Mg# vs $\varepsilon_{Nd}(t)$, b. Nb/La vs $\varepsilon_{Nd}(t)$, c. Si/P vs (Fe+Mg)/P and Eu* vs CaO plots. In the Mg# vs $\varepsilon_{Nd}(t)$ diagrams, a primary group 1 magma is assumed. The final composition variations of this group rocks resulted from both FC processes and input of juvenile melts of enriched mantle. Mineral abbreviations are Pl = plagioclase and Cpx = clinopyroxene. See text for further explanation.

show Eu/Eu* negative anomalies. Thus, the data suggest that the group 1 and 2 magmas originated from different source rocks. There appears to be a degree of decoupling between the Pb and Sr isotope systems, on the one hand, and the Nd system on the other. This may be due to the effects of metasomatic fluids on the magma's source rocks (see e.g. Conceição et al., 2005).

Group 1 granitoids are depleted in Y (<10.9 ppm) and HREE (e.g. Yb<0.8 ppm) and enriched in Sr (up to 812 ppm), with negative Nb and Ta anomalies in primitive mantle-normalized multi-element diagrams (Fig. 5a). They have high $(La/Yb)_N$ ratios (32 to 105) and Sr/Y ratios (43 to 92). Their isotopic features ($(^{87}Sr/^{86}Sr)_i > 0.705$, $\varepsilon_{Nd}(t) = -1.01$ to -6.12) suggest that their dominant protoliths were meta-igneous crustal rocks. These geochemical signatures are comparable to those of TTG rocks and adakites (Defant and Drummond, 1990). Nevertheless, with the exception sample TA-1, the group 1 rocks are all high-K series, with K_2O/Na_2O ratios ≈1, similar to the K-adakites of eastern China (Zhang et al., 2001; Rapp et al., 2002) and the Tibetan Plateau (Chung et al., 2003; Hou et al., 2004; Wang et al., 2005).

Several models have been proposed for the origin of adakitic magmas: partial melting of the oceanic slab, related to incipient subduction (Defant and Drummond, 1990; Peacock et al., 1994; Drummond et al., 1996; Sajona et al., 2000), partial melting of a slab undergoing low-angle subduction (Gutscher et al., 2000; Beate et al., 2001), partial melting of underplated basaltic lower crust (Muir et al., 1995; Barnes et al., 1996; Petford and Atherton, 1996; Xu et al., 2002), partial melting of lower crust thickened by continent–continent collision (Chung et al., 2003; Hou et al., 2004), and AFC processes (Castillo et al., 1999).

Experimental studies have shown that the magma sources for normal Na-rich adakites are probably basalts metamorphosed to garnet amphibolites and/or amphibole eclogites, at pressures equivalent to crustal thicknesses >40 km (Sen and Dunn, 1994; Rapp et al., 1999). Garnet is a major residual phase during partial melting of such sources, and this produces the typical HREE depletion in the melts. Thus, crustal thickening or partial melting of deep crustal rocks is essential for the generation of adakitic magmas that have crustal isotope signatures (such as those in the present study). New experimental results (Xiao and Clemens, 2007) suggest that the formation of K-adakite melts (lacking Eu anomalies) requires very high pressures (>2.0 GPa, equivalent to crustal thicknesses >66 km), together with high temperatures (>1075 °C). Additionally, it appears that the source rocks must be more potassic (higher K_2O/Na_2O) and more felsic than the basaltic protoliths of normal adakitic magmas. In the present study area, some group 1 adakites have small negative Eu anomalies (e.g. JL5 and JL6, Table 2, Fig. 5). This suggests that either there was some plagioclase in the residual source rocks or that the magmas experienced some plagioclase fractionation. The above discussion has demonstrated that the negative Eu anomalies most probably resulted from plagioclase fractionation, rather than from the presence of plagioclase in the residual source rocks (Fig. 8d). This suggests magma formation at depths of at least 66 km (Xiao and Clemens, 2007). In contrast, there are no corresponding relationships among the group 2 granitoids (Fig. 8d), suggesting their negative Eu anomalies were due to residual plagioclase in the source rocks. Thus, the group 2 I-type granitoids were probably formed by partial melting at pressures <1.7 GPa and most probably ≤1.5 GPa, where garnet is absent from the residue (Table 2 of Xiao and Clemens, 2007).

The group 1 granitoids have K_2O/Na_2O ratios of ≈1 (up to 1.59), low MgO contents (0.42 to 1.91 wt.%), Mg# (100×mol. MgO/[MgO+FeO])=27 to 45 and evolved Sr–Nd isotope compositions. Such characteristics distinguish the K-adakites from those adakites said to have been generated through partial melting of oceanic slabs (Defant and Drummond, 1990; Peacock et al., 1994; Drummond et al., 1996; Sajona et al., 2000) or underplated basaltic lower crust (Muir et al., 1995; Barnes et al., 1996; Petford and Atherton, 1996; Xu et al., 2002). Their slightly high initial $^{87}Sr/^{86}Sr$ values (mostly >0.706) and negative $\varepsilon_{Nd}(t)$ (-1.01 to -6.12) with $T_{DM}=0.94$ to 1.17 Ga, suggest that their magma source was predominantly Precambrian meta-igneous continental crust. A juvenile mantle contribution could be invoked, to explain their relatively young T_{DM} and higher $\varepsilon_{Nd}(t)$ values compared with group 2 I-type granitoids (Table 3). We suggest a model that involves continent–continent collision, crustal thickening and delamination and partial melting of the lower crust, to generate the group 1 K-adakite magmas. Some juvenile melts from the mantle may have mixed with the crustally derived adakitic melts. This interpretation is consonant with what is known about the convergence between the SGFB and the Qiangtang Block, in which the Songpan-Garzê Ocean was subducted westward along the Garzê-Litang suture (Mo et al., 1994; Sun et al., 1997; Li et al., 1999; Zhong, 2000; Roger et al., 2004; Reid et al., 2005). We argue that the closure of the Songpan-Garzê Ocean (probably a marginal sea) and crustal shortening during the Late Triassic (the "Indosinian Orogeny") thickened the crust of the SGFB to

>66 km, similar to the present-day Tibetan crust (which is up to 75 km thick).

5.2. Magma sources

There are two exposed candidate sources for the group 1 granitoid magmas. One is the Late Proterozoic Bikou Group of mafic metavolcanic rocks (~0.82 Ga, Yan et al., 2004), exposed in the NE of the SGFB. Another is the Proterozoic Kangding Complex (~0.7 Ga, Chen et al., 2000; 0.8 Ga, U–Pb zircon SHRIMP, Zhou et al., 2002), which forms the basement of the South China Block. The Bikou Group of metamorphic rocks can be ruled out because they have higher $\varepsilon_{Nd}(t)$=220 Ma (>0; Yan et al., 2004). The Xiao and Clemens (2007) experiments, also suggest that purely mafic sources would not be able to yield magmas with high enough K_2O/Na_2O. The major rocks in the Kangding Complex are Proterozoic TTGs. The Sr–Nd isotope compositions of the group 1 K-adakites overlap with those of the Kangding Complex (Fig. 7). Pb isotope data for the group 1 granitoids provide further evidence for the Yangtze (South China) affinity of the source rocks (Fig. 6). All group 1 rocks plot within the area defined by the Yangtze (South China) granitoids (Fig. 6), suggesting that they could have been generated from similar (or the same) source rocks. Derivation from TTG source rocks is in agreement with the experimental constraints summarised in Xiao and Clemens (2007).

Group 2 granitoids are ordinary, high-K, I-type granitoids (Figs. 3 and 4). Their geochemical features suggest that they were generated from sources containing some residual plagioclase but lacking garnet. This indicates lower pressures and depths <50 km for magma generation (Xiao and Clemens, 2007). Additionally, these group 2 rocks have older T_{DM} (1.20 to 1.87 Ga) and lower $\varepsilon_{Nd}(t)$ (−3.11 to −6.71) than the group 1 K-adakites. As both groups formed in same tectonic setting (i.e. the SGFB), these data suggest that the source rocks for the group 2 magmas must be older than the protoliths of the group 1 adakitic magmas. This might be seen as contradictory with the melting depth inferred from their geochemistry, since older source rocks might be expected to be found at deeper levels. However, this is apparently not the case here. There are two possible explanations. The complex thrust tectonics, that preceded the formation of the magmas, may have resulted younger crustal source materials being tectonically emplaced beneath older rocks. Alternatively, the Nd isotope system might have been modified by input of younger materials (e.g. juvenile magma from enriched mantle). The first model can be ruled out because, for the Early Triassic period, westward rather than eastward subduction along the Garzê-Litang suture has been confirmed (BGMR of Sichuan, 1990; Xu et al., 1992; Mo et al., 1994; Sun et al., 1997; Li et al., 1999; Zhong, 2000; Reid et al., 2005; Roger et al., 2004) and there was no tectonic underthrusting that could have resulted in young crustal material being emplaced beneath the old crust, prior to the magmatism. The second model is favoured by the isotope geochemistry. On the Pb isotope diagram (Fig. 6) and on the $(^{87}Sr/^{86}Sr)_i$ vs $\varepsilon_{Nd}(t=225\ Ma)$ diagram (Fig. 7), all granitoids plot within the area occupied by the rocks of the Kangding Complex and the Mesozoic South China granitoids. This implies that the Kangding Complex (or similar TTG-type rocks) could be the main protoliths for both of group 1 and group 2 granitoids. If so, there must have been very little juvenile mantle-derived melt involved in the group 2 magmas, though there is likely to have been some in the group 1 adakite magmas (Fig. 8a).

Group 2 granitoid magmas are likely to have formed by lower-*T* partial melting than group 1 magmas because group 1 have lower SiO_2 and higher MgO contents (Table 2, Fig. 3), requiring high temperatures. Production of the group 2 I-type magmas may also have involved quite high temperatures but this is more difficult to constrain. Their likely evolution at lower *P* (where H_2O is less soluble in the melts) means that substantial melt proportions could have been formed at lower *T* (e.g. Clemens and Vielzeuf, 1987).

5.3. Tectonic implications

Much attention has been paid to the study of the geological evolution of the SGFB and eastern Tibet, using geochronology and geochemistry (Roger et al., 2003, 2004; Reid et al., 2005; Qin et al., 2005; Zhang et al., 2006; Reid et al., in press). It is commonly accepted that the Jinshajiang Suture forms the boundary between the SGFB and the Qiangtang Block (Mo et al., 1993, 1994; Roger et al., 2003; Hou et al., 2004). However, recent work indicates that the boundary lies at the Garzê-Litang suture (Pan and Ding, 2005; Reid et al., 2005, in press). In the Late Triassic, collision occurred between the Yidun Arc and the SGFB, along the Garzê-Litang suture (BGMR of Sichuan, 1990). The data presented here provide further constraints on the tectonic setting and the geological evolution of eastern margin of the Tibetan Plateau.

Granitoids from northeast of the Garzê-Litang suture (SGFB) have geochemical and isotopic features distinct from those southwest of this structure. As mentioned earlier, the (group 1) K-adakite granitoids in the SGFB

have affinities with similar rocks from eastern China (Zhang et al., 2001; Rapp et al., 2002). Recently published geochemical data for the Maoergai, Yangon and Yushu intrusions, in the northern part of the SGFB, suggest that most of these are also K-adakites (Roger et al., 2003; Qin et al., 2005; Zhang et al., 2006). The western limit to the occurrence of the K-adakites is at the Garzê-Litang suture and the K-adakite province overlaps the SGFB, suggesting that all these magmatic rocks were generated in same tectonic setting. Furthermore, the time gap between collision (~244 Ma, Roger et al., 2003) and generation of these adakitic magmas (~225 Ma) suggests that collision produced thick crust that was stable for <20 Myr.

As discussed above, the very high pressures and temperatures that seem to be required for formation of K-adakite melts suggest magma generation by partial melting of delaminated, plagioclase-free, eclogitic, TTG-type crust within the mantle. An alternative scheme of lower crustal melting by heating of newly underplated basalts would not reproduce the chemistry of the K-adakitic rocks. The Emeishan mantle plume was active until the Late Permian (~258 Ma; Xiao et al., 2003; Zhou et al., 2005) but the time gap (~25 Myr) between these two magmatic events represents a further argument against this hypothesis. Melting of delaminated crust is the most likely scenario.

The SGFB was formed during the Indosinian Orogeny, and the closure of the Songpan Ocean (Xu et al., 1992). The spatial distribution of different geochemical varieties of granitoids suggests that the Garzê-Litang Ocean was subducted to the west and produced the Yidun-arc and Qiangtang block arc-type granitoids along the western side of the suture, extending over a length of 400 km. This is consistent with results of the structural study by Reid et al. (2005). The existence of the coeval K-adakite province implies that the SGFB crust had been thickened to an extent comparable with current Tibetan Plateau in the Late Triassic. Thus, the Garzê-Litang suture is a more important structure than the Jinshajiang suture, exerting greater control over regional tectonic evolution.

Our data also provide constraints on the nature of the basement of the SGFB. We have concluded that the source rocks for the granitoid magmas were similar to rocks of the Kangding Complex. This means that the Songpan-Garzê belt shared the same basement as the Yangtze (South China) Block.

In contrast to the tectonic setting typically assumed for adakites (partial melting of subducted oceanic crust distributed on the arc side over a mantle wedge) the SGFB is a collisional orogen constructed from a passive margin. The standard assumption about adakite genesis also differs from the case of eastern China and the Tibetan Plateau. K-adakites from eastern China formed in the Late Mesozoic (~130 Ma), have lower $\varepsilon_{Nd}(t)$ values (<−10) and older T_{DM} (1.8 to 2.2 Ga) (Zhang et al., 2001). They are interpreted as being related to extensive thinning and delamination of a previously thickened crust (Xu et al., 2002; Xiao et al., 2004; Gao et al., 2005). K-adakites from the Tibetan Plateau formed in the Cenozoic (at 30 to 10 Ma), by partial melting of thickened crust (up to 75 or 80 km) (Chung et al., 2003; Hou et al., 2004; Wang et al., 2005). Thus, collisional and thickened continental crust can form the source of K-rich adakitic magmas. Although this paper describes the oldest known non-arc and K-rich adakites, such rocks may well be present other older orogens or regions of thickened continental crust.

6. Conclusions

Late Triassic granitoids from the SGFB on eastern margin of the Tibetan Plateau show distinctive geochemical and isotopic characteristics. This study provides the following constraints on their petrogenesis and tectonic significance:

1) The Late Triassic granitoids here are coeval and I-type, but sourced from different crustal regions (depths).
2) Granitoids from the SGFB were can be divided into two groups. Group 1 have K-adakite affinities while group 2 are ordinary high-K, I-type granitoids. The group 1 K-adakites are products of partial melting of delaminated collisional and thickened TTG lower crust, with a small admixture of juvenile melt from enriched mantle. Group 2 magmas were generated through partial melting of relatively shallower crust, possibly of similar character.
3) The basement of the SGFB has geochemical and isotopic features similar to the Kangding Complex, suggesting that the Belt was constructed from the same sorts of rocks as the basement of South China.
4) This area was greatly thickened (up to 66 km) during the early stage of the Indosinian orogeny (~244 Ma) and then the lower crust delaminated within a very short time (<20 Myr).

Acknowledgments

This study was financially supported by the Natural Science Foundation of China (40234052 and 40572031) and the Geological Survey Party of Sichuan Province. A Royal Society International Outgoing Short Visit to China facilitated JDC's contribution.

References

Barnes, C.G., Petersen, S.W., Kistler, R.W., Murray, R., Kay, M.A., 1996. Source and tectonic implications of tonalite–trondhjemite magmatism in the Klamath Mountain. Contrib. Mineral. Petrol. 123, 40–60.

Beate, B., Monzier, M., Spikings, R., Cotton, J., Silva, J., Bourdon, E., Eissen, J.P., 2001. Mio–Pliocene adakite generation related to flat subduction in southern Ecuador: the Quimsacocha volcanic centre. Earth Planet. Sci. Lett. 192, 561–570.

BGMR (Bureau of Geology and Mineral Resources) of Sichuan Province, 1990. Regional Geology of Sichuan Province, vol. 21. Geological Publishing House, Beijing, pp. 1–745 (in Chinese with English abstract).

Bruguier, O., Lancelot, J.R., Malavieille, J., 1997. U-Pb dating on single zircon grains from the Triassic Songpan-Garze flysch (Central China): Provenance and tectonic correlations. Earth Planet. Sci. Lett. 152, 217–231.

Calassou, S., 1994. Étude tectonique d'une chaine de décollement: A) tectonique Triasique et Tertiaire de la chaine de Songpan-Garzê. B) géométrie et cinématique des déformations dans les prismes d'accrétion sédimentaire: modélisation analogique. PhD Thesis, Univ. Montpellier II, pp. 1-400.

Castillo, R.P., Janney, P.E., Solidum, R.S., 1999. Petrology and geochemistry of Camiguin Island, southern Philippines: insight to the source of adakites and other lavas in a complex arc setting. Contrib. Mineral. Petrol. 134, 33–51.

Chappell, B.J., White, A.J.R., 1974. two Contrasting granite types. Pac. Geol. 8, 173–174.

Chappell, B.W., White, A.J.R., 2001. Two contrasting granite types: 25 years later. Aust. J. Earth Sci. 48, 489–499.

Chen, S.F., Wilson, C.J.L., 1996. Emplacement of the Longmen Shan Thrust—Nappe Belt along the eastern margin of the Tibetan Plateau. J. Struct. Geol. 18, 413–440.

Chen, S.F., Wilson, C.J.L., Worley, B.A., 1995. Tectonic transition from the Songpan-Garzê Fold Belt to the Sichuan Basin, southwestern China. Basin Res. 7, 235–253.

Chen, Y.L., Luo, Z.H., Liu, C., 2000. Re-recognition on the western margin of the Yangtze craton based on Nd and Pb isotopic compositions. Eos, AGU Western Pacific Geophysics Meeting, Suppl. 81, p. 32B-03.

Chung, S.L., Liu, D., Ji, J., Chu, M.F., Lee, H.Y., Wen, D.J., Lo, C.H., Lee, T.Y., Qian, Q., Zhang, Q., 2003. Adakites from continental collision zones: melting of thickened lower crust beneath southern Tibet. Geology 31, 1021–1024.

Clemens, J.D., Vielzeuf, D., 1987. Constraints on melting and magma production in the crust. Earth Planet. Sci. Lett. 86, 287–306.

Conceição, R.V., Mallmann, G., Koester, E., Schilling, M., Bertotto, G.W., Rodriguez-Vargas, A., 2005. Andean subduction-related mantle xenoliths: isotopic evidence of Sr–Nd decoupling during metasomatism. Lithos 82, 273–287.

Defant, M.J., Drummond, M.S., 1990. Derivation of some modern arc magmas by melting of young subducted lithosphere. Nature 34, 662–665.

Drummond, M.S., Defant, M.J., Kepezhinskas, P.K., 1996. Petrogenesis of slab-derived trondhjemite–tonalite–dacite/adakite magmas. Trans. R. Soc. Edinb. Earth Sci. 87, 205–215.

Elena, A.K, Maurice, B., Jacques, M., 2003. Discovery of the Tethys–Tethys residual peridotites along the Anyemaqen–KunLun suture zone (North Tibet). C. R. Geoscience 335, 709–719.

Enkin, R., Yang, Z., Chen, Y., Courtillot, V., 1992. Paleomagnetic constraints on the geodynamic history of the major blocks of China from the Permian to the present. J. Geophys. Res. 97, 13953–13989.

Ernst, R.E., Fowler, A.D., Pearce, T.H., 1988. Modelling of igneous fractionation and other processes using Pearce diagrams. Contrib. Mineral. Petrol. 100, 12–18.

Gao, S., Rudnick, R.L., Yuan, H.L., Liu, X.M., Liu, Y.S., Liu, W.L., Ayers, J., Wang, X.C., Wang, Q.H., 2005. Recycling lower continental crust in the North China craton. Nature 432, 892–897.

Gutscher, M.A., Maury, R., Eissen, J.P., Bourdon, E., 2000. Can slab melting be caused by flat subduction? Geology 28, 535–538.

Harrowfield, M.J., Wilson, C.J.L., 2005. Indosinian deformation of the Songpan Garzê Fold Belt, northeast Tibetan Plateau. J. Struct. Geol. 27, 101–117.

Hou, Z.Q., Gao, Y.F., Qu, X.M., Rui, Z.Y., Mo, X.X., 2004. Origin of adakitic intrusives generated during mid-Miocene east–west extension in southern Tibet. Earth Planet. Sci. Lett. 220, 139–155.

Li, X., Liu, W., Wang, Y., Zhu, Q., Du, D., Shen, G., Liu, C., Que, M., Yang, S., 1999. The Tectonic Evolution and Metallogenesis in the Tethys of the Nujiang–Lancangjiang–Jinshajiang Area, Southwestern China. Geological Publishing House, Beijing. (in Chinese).

Liang, X.R., Wei, G.J., Li, X.H., Liu, Y., 2003. Precise measurement of $^{143}Nd/^{144}Nd$ and Sm/Nd ratios using multiple-collectors inductively coupled plasma-mass spectrometer (MS-ICPMS). Geochemica 32, 91–96.

Liu, Y., Liu, H.C., Li, X.H., 1996. Simultaneous and precise determination of 40 trace elements in rock samples using ICP-MS. Geochemica 25, 552–558.

Ma, L.F. (Ed.), 2002. China Geological Atlas. Geological Publishing House, Beijing, pp. 278–279.

Mattauer, M., Malavieille, J., Calassou, S., Lancelot, J., Roger, F., Hao, Z., Xu, Z., Hou, L., 1992. La chaîne triasique de Songpan-Garze (Quest Sechuan et Est Tibet): une chaîne de plissement-décollement sur marge passive. Comptes Rendus de l'Académie des Sciences Paris 314, 619–626.

Mo, X.X., et al., 1993. Sanjiang Tethyan Volcanism and Related Mineralization. Geological Memories, Series 3, No. 20. Geological Publishing House, Beijing, pp. 1–267.

Mo, X.X., Deng, J.F., Lu, F., 1994. Volcanism and the evolution of Tethys in Sanjiang area, southwestern China. In: Metcalfe, I. (Ed.), Gondwana Dispersion and Asian Accretion. Proceedings of the First International Symposium, IGCP Project 321 Journal of Southeast Asian Earth Sciences, vol. 9(4). Pergamon, Oxford, UK, pp. 325–333.

Muir, R.G., Weaver, S.D., Bradshaw, J.D., Eby, G.N., Evans, J.A., 1995. Geochemistry of the cretaceous separation point batholiths, New Zealand: granitoid magmas formed by melting of mafic lithosphere. J. Geol. Soc. (London) 152, 689–701.

Pan, G.T., Ding, J., 2005. Geological Map of the Tibetan Plateau and Adjacent Areas (1: 1,500,000). Chengdu Map Publishing House, Chengdu.

Peacock, S.M., Rusher, T., Thompson, A.B., 1994. Partial melting of subducting oceanic crust. Earth Planet. Sci. Lett. 121, 224–227.

Petford, N., Atherton, M., 1996. Na-rich partial melts from newly underplated basaltic crust: the Cordillera Blanca batholith, Peru. J. Petrol. 37, 1491–1521.

Qin, J.F., Lai, S.C., Li, Y.F., 2005. Petrogenesis and geological significance of Yangba granodiorites from Bikou area Northern margin of Yangtze Plate. Acta Petrol. Sin. 21, 697–710.

Rapp, P.R., Shimizu, N., Norman, M.D., Applegate, G.S., 1999. Reaction between slab-derived melt and peridotite in the mantle

wedge: experimental constrains at 3.8 GPa. Chem. Geol. 160, 335–356.

Rapp, P.R., Xiao, L., Shimizu, N., 2002. Experimental constraints on the origin of potassium-rich adakites in eastern China. Acta Petrol. Sin. 18, 293–302.

Reid, A.J., Wilson, C.J.L., Liu, S., 2005. Structural evidence for the Permo–Triassic tectonic evolution of the Yidun arc, eastern Tibetan Plateau. J. Struct. Geol. 27, 119–137.

Reid, A.J., Wilson, C.J.L., Liu, Sun., Pearson, N., Belousova, E., in press. Mesozoic plutons of the Yidun Arc, SW China: U/Pb geochronology and Hf isotopic signature. Ore Geol. Rev.

Roger, F., Calassou, S., Lancelot, J., Malavieille, J., Mattauer, M., Xu, Z.Q., Hao, Z.W., Hou, L.W., 1995. Miocene emplacement and deformation of the Konga Shan granite (Xianshui He fault zone, west Sichuan, China): geodynamic implications. Earth Planet. Sci. Lett. 130, 201–216.

Roger, F., Arnaud, N., Gilder, S., Tapponnier, P., Jolivet, M., Brunel, M., Malavieille, J., Xu, Z., 2003. Geochronological and geochemical constraints on Mesozoic suturing in East Central Tibet. Tectonics 22, 111–119.

Roger, F., Malavieille, J., Leloup, P.H., Calassou, S., Xu, Z., 2004. Timing of granite emplacement and cooling in the Songpan-Garzê Fold Belt (eastern margin of the Tibetan Plateau) with tectonic implications. J. Asian Earth Sci. 22, 465–481.

Sajona, F.G., Maury, R.C., Pubellier, M., 2000. Magmatic source enrichment by slab-derived melts in a young post-collision setting, central Mindanao (Philippines). Lithos 54, 173–206.

Sen, C., Dunn, T., 1994. Dehydration melting of a basaltic composition amphibolite at 1.5 and 2.0 GPa: implication for the origin of adakites. Contrib. Mineral. Petrol. 117, 394–409.

Sengör, A.M.C., 1984. The cimmeride orogenic system and the tectonics of Eurasia. Spec. Pap.-Geol. Soc. Am. 195.

Sengör, A.M.C., 1985. Tectonic subdivisions and evolution of Asia. Bull. Tech. Univ. Istanbul 46, 355–435.

Sun, X., Zhang, B., Nie, Z., Liang, D., 1997. Formation, age and environment of ophiolite and ophiolitic melange in the Jinshajiang Belt, northwestern Yunnan. Geol. Rev. 43, 113–120 (in Chinese with English abstract).

Sun, Y., Chen, L., Fen, G.T., Gao, M., He, Y.H., 2002. A dynamic model of Paleo-Tethyan evolution: evidences from Paleo-Tethyan ophiolite in China. J. Northwest University 32, 1–6 (in Chinese with English abstract).

Wang, Q., McDermott, F., Xu, J.F., Bellon, H., Zhu, Y.T., 2005. Cenozoic K-rich adakitic volcanic rocks in the Hohxil area, northern Tibet: lower-crustal melting in an intercontinental setting. Geology 33, 465–468.

Xiao, L., Clemens, J.D., 2007. Origin of potassic (C-type) adakite magmas: experimental and field constraints. Lithos 95, 399–414.

Xiao, L., Xu, Y.G., Chung, S.L., He, B., Mei, H.J., 2003. Chemostratigraphic correlation of Upper Permian lavas from Yunnan Province, China: extent of the Emeishan large igneous province. Int. Geol. Rev. 45, 753–766.

Xiao, L., Rapp, R.P., Xu, J.F., 2004. The role of deep processes controls on variation of compositions of adakitic rocks. Acta Petrol. Sin. 20, 219–228.

Xu, Z., Hou, L., Wang, Z., 1992. Orogenic Processes of the Songpan-Garzê Orogenic Belt of China. Geological Publishing House, Beijing, pp. 1–190.

Xu, J.F., Shinjo, R., Defant, M.J., Wang, Q., Rapp, R.P., 2002. Origin of Mesozoic adakitic intrusive rocks in the Ningzhen area of east China: partial melting of delaminated lower continental crust? Geology 30, 1111–1114.

Yan, Q.R., Andrew, D.H., Wang, Z.Q., Yan, Z., Liu, D.Y., Song, B.L., Jiang, C.F., 2004. Geochemistry and tectonic setting of the Bikou volcanic terrain on the northern margin of the Yangtze plate. Acta Petrol. Mineral. 23, 1–11.

Yin, A., Nie, S., 1993. An indentation model for the North and South China collision and the development of the Tan-Lu and Honam Fault Systems, Eastern Asia. Tectonics 12, 801–813.

Yuan, H.L., Gao, S., Liu, X.M., Li, H.M., Gunther, D., Wu, F.Y., 2004. Accurate U–Pb age and trace element determinations of zircon by laser ablation-inductively coupled plasma-mass spectrometry. Geostand. Geoanal. Res. 28, 353–370.

Zartman, R.E., Doe, B.R., 1981. Plumbotectonics — the model. Tectonophysics 75, 135–162.

Zhang, L.G., 1995. Block-Geology of Eastern Asia Lithosphere—Isotope Geochemistry and Dynamics of Upper Mantle, Basement and Granite. Chinese Science Press, Beijing, p. 252 (in Chinese with English abstract).

Zhang, Q., Wang, Y., Wang, Y.L., 2001. Preliminary study on the components of the lower crust in east China Plateau during Yanshanian period: constraints on Sr and Nd isotopic compositions of adakite-like rocks. Acta Petrol. Sin. 17, 505–513.

Zhang, H.F., Zhang, L., Harris, N., Jin, L.L., Yuan, H.L., Zhang, B.R., 2006. U-Pb zircon ages, geochemical and isotopic compositions of granitoids in Songpan-Garzê Fold Belt, eastern Tibet Plateau: constraints on petrogenesis, nature of basement and tectonic evolution. Contrib. Mineral. Petrol. 152, 75–88.

Zhang, H.F., Xiao, L., Zhang, L., Yuan, H.L., Jin, L.L., in press, Geochemical and Pb–Sr–Nd isotopic compositions of Indosinian granitoids from the Bikou block, northwest of the Yangtze plate: constraints on petrogenesis, nature of deep crust and geodynamics. Science in China.

Zhong, D., 2000. Palaeotethysides in West Yunnan and Sichuan, China. Science Press, Beijing. (in Chinese with English abstract).

Zhou, M.F., Yan, D.P., Kennedy, A.K., 2002. SHRIMP U–Pb zircon geochronological and geochemical evidence for Neoproterozoic arc-magmatism along the west margin of the Yangtze Block, South China. Earth Planet. Sci. Lett. 196, 51–67.

Zhou, M.F., Zhao, J.H., Qi, L., Su, W.C., Hu, R.Z., 2005. Zircon U–Pb geochronology and elemental and Sr–Nd isotope geochemistry of Permian mafic rocks in the Funing area, SW China. Contrib. Mineral. Petrol. 151, 1–19.